Journal of Physics: Conference Series

PAPER • OPEN ACCESS

Beam dynamics optimization for high gradient beam driven plasma wakefield acceleration at SPARC-LAB

To cite this article: M. Carillo *et al* 2024 *J. Phys.: Conf. Ser.* **2687** 062023

Journal of Physics: Conference Series **2687** (2024) 062023 doi:10.1088/1742-6596/2687/6/062023

Beam dynamics optimization for high gradient beam driven plasma wakefield acceleration at SPARC-LAB

M. Carillo[1,4],D. Alesini[2], M. P. Anania[2], M. Behtouei[2], M. Bellaveglia[2], A. Biagioni[2] , E. Chiadroni[1,2], A. Cianchi[5,2], G. Costa[2], L. Crincoli[1,2], A. Del Dotto[2], M. Del Giorno[2],G. Di Pirro[2], L. Faillace[1,2], D. Francescone[1], M. Galletti[5,2], L. Giannessi[2], A. Giribono[2], L. Giuliano[1,4], P. Iovine[1,2], A. Mostacci[1,4], V. Petrillo[2], R. Pompili[2], G. Parise[5], S. Romeo[2], A. R. Rossi[6], G. J. Silvi[1,4], V. Shpakov[2],C. Vaccarezza[2], F. Villa[2], M. Ferrario[2]

[1]Sapienza University of Rome, 00161 Rome, Italy
[2]INFN-LNF, 00044 Frascati, Italy
[3]UCLA, Los Angeles, 90095 California, USA
[4] INFN-Sez.Roma1, 00161 Roma, Italy
[5] University of Rome Tor Vergata, Rome, Italy
[6] INFN-Milano, Milano, Italy

E-mail: martina.carillo@uniroma1.it

Abstract.
The SPARC_LAB test facility at the LNF (Laboratori Nazionali di Frascati, Rome) holds a high brightness photo-injector used to investigate advanced beam manipulation techniques. High brightness electron bunch trains (so-called comb beams) can be generated striking on the photo-cathode of a Radio Frequency (RF) photo-injector with a ultra-short UV laser pulse train in tandem with the velocity bunching technique. Beam dynamics studies have been performed with the aim of optimizing the dynamics of the double beam (driver and witness) used to perform particle driven plasma wake field acceleration (PWFA). In this scenario different scans on beam parameters were carried on adopting the ASTRA simulation code, in order to optimize the witness beam quality and improve the plasma booster stage performances. A benchmark of the simulations has been then performed, reproducing the experimental data obtained from the optimization of machine performances, and a good agreement was found.

1. INTRODUCTION

Plasma wakefield acceleration, proposed in 1979 by Tajima & Dawson [1], has attracted much attention due to the possibility of generating large acceleration using laser pulses or charged particle beams. This could allow for ultracompact accelerators for a wide range of many applications including free electron laser (FEL) [2, 3], Compton scattering [4], THz radiation[5, 6], and medical and industrial uses. However, the further development of plasma-based sources requires improvement in beam quality, specifically energy spread and emittance. SPARC_LAB [7] focuses on creating high-quality electron beams using plasma-based acceleration experiments, resulting in the first Free-Electron Laser lasing from a beam driven plasma-accelerated electron beam [8, 9, 10]. The SPARC_LAB photoinjector consists of an electron

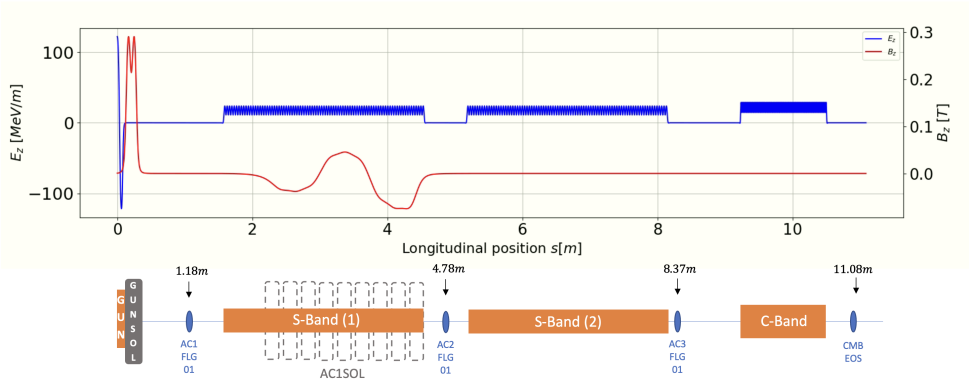

Figure 1: Top plot: electric (blue) and magnetic (red) fields of accelerator cavities. Lower plot: schematic of SPARC_LAB photoinjector with gun, sections, solenoids, and reference cameras.

gun and three accelerating sections and solenoids. The developments are motivated by the EuPRAXIA@SPARC LAB [11] user facility project, aiming to develope the first plasma beam-driven user facility at LNF[12]. Figure 1 shows the layout used in the present experimental setup.

SPARC_LAB operational mode involves impinging on the photocathode with a comb-shaped laser pulse, resulting in a series of high-charge density pulses that are less than hundred femtosecond in duration. These pulses are generated within the same bucket of the RF gun accelerator. As the pulses move downstream from the gun exit, the space charge force causes a linear energy chirp to develop along each pulse. This chirp can be used to compress the original charge profile by utilizing the first RF accelerating structure working on velocity bunching mode [13].

2. Beam dynamics data benchmark

The SPARC photo-injector [14, 15] is an advanced system capable of producing electron beams with varying charge and duration, as well as peak current. Despite its high level of flexibility, the injector maintains a high-quality beam with relatively small projected emittances, enabling precise control over beam properties for different experiments and applications. In this study, we examine the behavior of the comb beam used for the last experimental campaign performed at SPARC_LAB, whose results are reported in [16], devoted to increase the efficiency of the plasma accelerator module already measured in [8]. The idea is to increase the driver and the witness charge. In details, we study the case of a driver beam with a charge of 500 pC and a witness beam with a charge of 50 pC, both generated using a copper cathode. The driver beam is produced with a uniform laser with an initial rms radius of 500 μm and 230 μm respectively Both beams exhibit a Gaussian longitudinal duration of about 100 fs, with the two bunches showing an initial delay of 3.5 ps. To explore the beam dynamics in the high-brightness photo-injector at SPARC_LAB, we conducted simulations using the ASTRA code [17]. This code takes into account space charge effects, which are relevant at very low energies, as well as thermal emittance. However, during the data acquisition, the two beams were not detected separately in the transverse plane. Then, to compare experimental data with simulations, we used the same image analysis process used in the control room to analyze the latter. The results of the comparison between simulations and experimental data are presented in Table 1, where we report in each column the output data from the simulation, the experimental data acquired from the downstream the third accelerating structure, and the percentual error between the

simulation and experimental data.

Table 1: Simulation and Experimantal Data Comparison

	Simulation	**Data**	**Error** [%]
E [MeV]	95.4	96.44± 0.38	1.1
ε_x [μ mrad]	6.8	10.0 ± 3.18	32.0
ε_y [μ mrad]	6.8	6.05± 2.55	4.6
σ_z [fs]	570	545	4.6
Δt [ps]	1.05	1.10	4.5

The comparison of experimental and simulated data for the majority beam parameters in a particle accelerator reveals a good overall agreement, except for the horizontal emittance. The disagreement shown in the horizontal emittance is attributed to a misalignment of the machine stages in the horizontal plane. Specifically, misalignments are not accounted for in the simulations as well as they do not consider any potential asymmetries in the cathode that may cause a deviation between the vertical and horizontal planes.

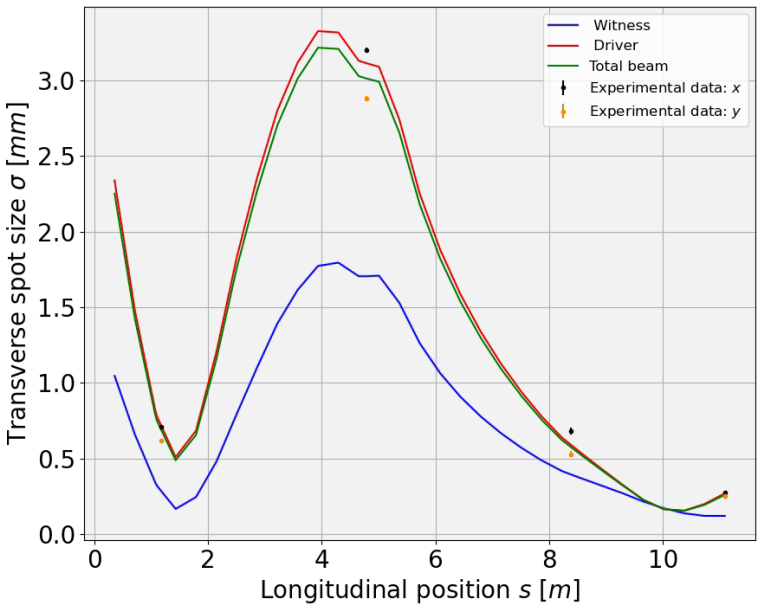

Figure 2: Position-dependent behavior of the SPARC photo-injector beams. Black and orange dots with error bars indicate experimental x and y data, respectively, while the green, red, and blue curves represent the transverse envelopes of the total, driver, and witness beams.

The data presented in Fig. 2 depict the total beam envelopes extracted along the machine. Notably, the comparison between the simulated and experimental data shows a satisfactory level of agreement. The total beam envelope, indicated by the green curve, accurately reproduces the experimental data. However, there is a discernible mismatch between the horizontal and vertical planes, which may arise from potential cathode asymmetries and/or misalignment in the horizontal plane, as indicated by the experimental observations we did above. In Table 2, we report the numerical comparison between the data obtained from the simulation and the

experimental data for each position. In the third column, the percentage error that the simulation makes compared to the experimental data has been calculated.

Table 2: Total Beam Envelope Data Analysis: all data are in [mm]

	Simulation	**Data**	**Error** [%]
AC1 x	0.680	0.712 ± 0.011	4.5
AC1 y	0.680	0.620 ± 0.011	9.7
AC2 x	3.022	3.200 ± 0.017	5.6
AC2 y	3.022	2.880 ± 0.013	4.9
AC3 x	0.580	0.683 ± 0.023	15.1
AC3 y	0.580	0.529 ± 0.021	5.1
EOS x	0.257	0.273 ± 0.011	5.9
EOS y	0.257	0.250 ± 0.005	2.8

Based on the values presented in Table 2, it can be concluded that the simulated envelope effectively replicates the experimental data within an acceptable range of error. However, the simulation results for AC3x exhibit a larger discrepancy compared to the experimental data, which is likely attributed to measurement jitter or misalignment between witness and driver that could be amplified by the first section solenoid. In addition to reproduce the experimental data of the total beam, the simulation also provides the dynamics of the individual beams: witness and driver, as observed in Fig. 2.

3. Comb Beam parameters Scan

After reproducing the results obtained from the machine with sufficient accuracy, the goal of the simulation work was to identify an operating point that would optimize the beams. To improve the performance of injection into the plasma acceleration section and to obtain a high-brightness electron beam output from the entire machine, the Witness and Driver must satisfy the parameter range shown in the Table 3. To optimize the dynamics of the Witness and Driver beams, a parameter scan was performed on the initial spot sizes ($\sigma_{x,W}(0)$ and $\sigma_{x,D}(0)$) and the initial cathode distance between the two beams ($\Delta t(0)$). During the scan the remaining parameters, such as solenoid magnetic field and sections phase, were kept constant to isolate their direct impact. The transverse emittance of the Witness beam was investigated as a function of the initial Driver spot size for different initial Witness spot sizes, as shown in Fig. 3.

Table 3: Range of Values for Optimization Parameters

	Witness	**Driver**
Transverse Emittance [μ mrad]	$[0, 1]$	None
α Twiss	$[-1, 0]$	$[-2, 0]$
β Twiss [m]	$[0, 10]$	$[0, 10]$
Bunch length σ_z[fs]	< 100	¡450
W-D Distance Δt[ps]	$[1, 1.6]$	

This shows that the emittance of the witness decreases as the initial transverse spot size of the driver increases. This can be attributed to the witness experiencing weaker space charge forces as it passes through the less dense driver during longitudinal compression as already illustrated in [18]. This idea is here supported by observing the evolution of the individual envelopes for

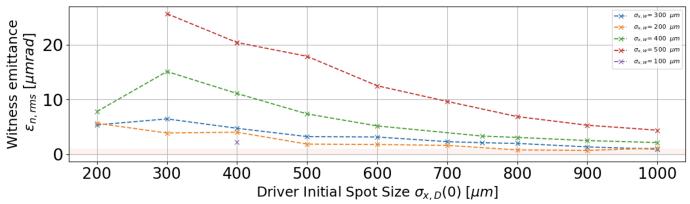

Figure 3: Transverse rms emittance of the Witness beam depends on the initial spot size of the Driver beam., for different initial spot size of the Witness beam. The acceptable parameter range is highlighted in red shaded area.

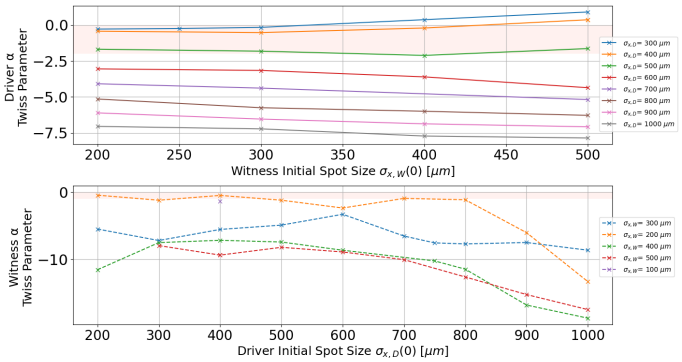

(a) Alpha Twiss Parameter

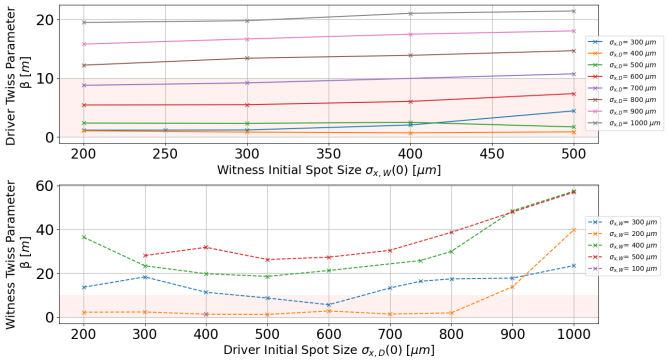

(b) Beta Twiss parameter

Figure 4: Twiss parameter for the Witness and Driver beams versus their initial spot sizes. The red shaded regions indicate acceptable parameter ranges as defined in Table 3.

the different cases examined. In fact, by varying the charge density of the driver, the position at which the witness reaches a transverse waist also varies along the machine. Additionally, the crossed Twiss parameters were analyzed to assess their variation throughout the parameter scan and shown in Figs. 4a and 4b. Indeed, these parameters have a significant importance in the dynamics of entering the permanent quadrupoles.

In both cases, it is clear that the driver does not exhibit significant changes with respect to

the witness' $\sigma(0)$. This effect was also observed for other parameters analyzed, such as beam length and emittance. The reason for this can be attributed to the charge carried by the driver (500 pC) being much greater than that of the witness (50 pC). As a result, the dynamics of the driver is not significantly impacted by the presence of the smaller beam. In Fig. 5, we plot the distance between the Witness and Driver beams as a function of the initial $\sigma_x(0)$ of the Driver. The results show that larger initial radii of the driver beam result in the two beams exiting the accelerator system closer together. This can be explained by the weaker spatial charge forces between the beams due to lower charge densities and by the image charge forces at the cathode as it scales as $1/r^2$. All these hypothesis are confirmed by the distance variation along the machine for different cases.

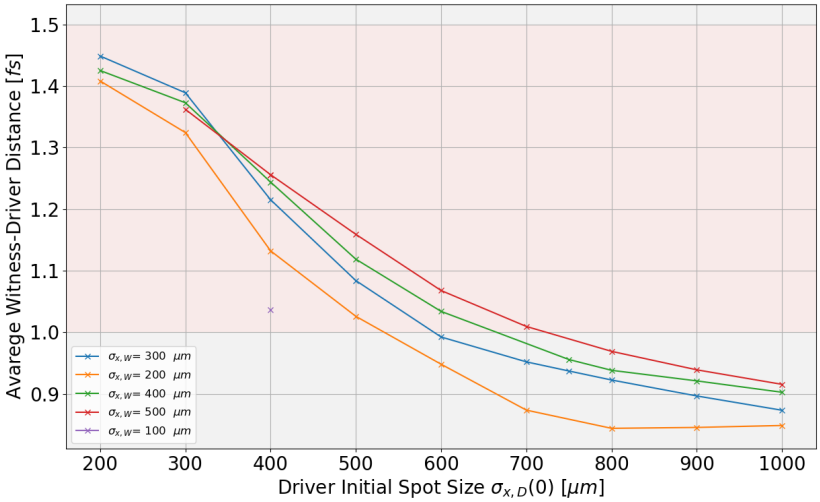

Figure 5: Witness-Driver distance as function of the initial driver spot size, for different initial witness spot size. The red shaded regions indicate acceptable parameter ranges as defined in Table 3.

4. CONCLUSION

In conclusion, a good agreement between the ASTRA simulations and experimental data has been found. A scan of the beam dynamics parameters was performed to optimize the injection beams into the plasma. The initial spot sizes that optimize the dynamics were found to be $\sigma_{x,W}(0)$=200 μm, $\sigma_{x,D}(0)$=400 μm, and an initial distance of Δt= 3.0 ps. Further scans on other parameters will be performed to better optimize machine performance and try to minimize the emittance of the witness in the range of acceptable values.

References

[1] T. Tajima, and J. M. Dawson, "Laser Electron Accelerator", *Phys. Rev. Lett.*, vol. 43, no. 4, p. 267, Jul. 1979. doi:10.1103/PhysRevLett.43.267,

[2] J. B. Rosenzweig *et al.*, "An ultra-compact x-ray free-electron laser", *New J. Phys.*, vol. 22, Sep. 2020. doi:10.1088/1367-2630/abb16c

[3] A. R. Rossi *et al.*, "Plasma boosted electron beams for driving Free Electron Lasers", *Nucl. Instrum. Methods Phys. Res. Sect. A*, vol. 909, pp. 54–57, 2018. doi:10.1016/j.nima.2018.02.092

[4] F. V. Hartemann *et al.*, "Compton scattering x-ray sources driven by laser wakefield acceleration", *Phys. Rev. Spec. Top. Accel. Beams* vol. 10, p. 011301, Jan. 2007, doi:10.1103/PhysRevSTAB.10.011301

[5] E. Chiadroni *et al.*, "A Versatile THz Source from High-Brightness Electron Beams: Generation and Characterization", *Condens. Matter* vol. 5, no. 2, p. 40, Jun. 2020. doi:10.3390/condmat5020040

[6] J. A. Fülöp, S. Tzortzakis, T. Kampfrath, "Laser-Driven Strong-Field Terahertz Sources", *Adv. Optical Mater*, vol. 8, p. 1900681, 2020, doi:10.1002/adom.201900681
[7] SPARC LAB, https://sparclab.lnf.infn.it/, 2023.
[8] R. Pompili *et al.*, "Energy spread minimization in a beam-driven plasma wakefield accelerator", *Nat. Phys.*, vol. 17, pp. 499–503, Jan. 2021. doi:10.1038/s41567-020-01116-9
[9] M. Galletti *et al.*, "Stable Operation of a Free-Electron Laser Driven by a Plasma Accelerator", *Phys. Rev. Lett.*, vol. 129, p. 234801, Nov. 2022 doi:10.1103/PhysRevLett.129.234801
[10] R. Pompili *et al.*, "Free-electron lasing with compact beam-driven plasma wakefield accelerator, *Nature*, vol. 605, pp. 659–662, May 2022. doi:10.1038/s41586-022-04589-1
[11] R. W. Assmann *et al.*, "EuPRAXIA Conceptual Design Report", *Eur. Phys. J. Spec. Top.*, vol. 229, pp. 3675–4284, Dec. 2020. doi:10.1140/epjst/e2020-000127-8
[12] M. Ferrario *et al.*, "EuPRAXIA@SPARC_LAB:Design study towards a compact FEL facility at LNF", *Nucl. Instrum. Methods Phys. Res. Sect. A*, vol. 909, pp. 134–138, Nov. 2018. doi:10.1016/j.nima.2018.01.094
[13] L. Serafini and M. Ferrario, "Velocity bunching in photo-injectors", *AIP Conf. Proc.*, vol. 581, no. 1, pp. 87–106, Aug. 2001. doi:10.1063/1.1401564
[14] D. Alesini *et al.*, "The SPARC project: a high-brightness electron beam source at LNF to drive a SASE-FEL experiment", *Nucl. Instrum. Methods Phys. Res. Sect. A*, vol. 507, no 1–2, pp. 345–349, Jul. 2003. doi:10.1016/S0168-9002(03)00943-4
[15] V. Shpakov *et al.*, "Design, optimization and experimental characterization of RF injectors for high brightness electron beams and plasma acceleration", *J. Instrum.*, vol. 17, no.12, p. P12022, Dec. 2022. doi:10.1088/1748-0221/17/12/P12022
[16] A. Giribono *et al.*, "Recent experimental results on the particle driven acceleration at the SPARC_LAB test facility", presented at the IPAC'23, Venezia, Italy, May 2023, paper TUPL131, this proceedings.
[17] K. Floettmann, ASTRA, https://www.desy.de/~mpyflo/
[18] A. Giribono *et al.*, "EuPRAXIA@SPARC_LAB: The high-brightness RF photo-injector layout proposal", *Nucl. Instrum. Methods Phys. Res. Sect. A*, vol. 909, pp. 282–285, Nov. 2018. doi:10.1016/j.nima.2018.03.009